

Green Composite of Instant Coffee and Poly(vinyl alcohol): An Excellent Transparent UV-Shielding Material with Superior Thermal-Oxidative Stability

Yadong Lyu, Xiaohong Gu,* and Yimin Mao*

Cite This: *Ind. Eng. Chem. Res.* 2020, 59, 8640–8648

Read Online

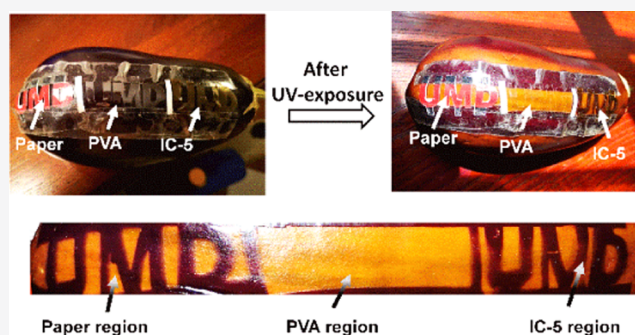
ACCESS |

Metrics & More

Article Recommendations

Supporting Information

ABSTRACT: Producing ultraviolet-light-shielding (UV-shielding) materials via green chemistry has been attracting researchers' attention. Herein, a polymer composite produced by hybridizing instant coffee with poly(vinyl alcohol) (PVA) is reported. It has been shown that adding coffee extract can significantly improve the UV-shielding property of the PVA material in the wavelength range between 200 and 400 nm, and the polymer composite remains largely transparent in the visible region. The UV-shielding performance of the composite can be maintained under the accelerated aging condition with a UV light dose of 40 MJ/m² for 68 h (approximately equivalent to a 45-day outdoor exposure in Miami, Florida). In addition, enhanced thermal-oxidative stability has been observed for the composite, as indicated in the thermal gravimetric analysis (TGA). The composite material can be used in the form of polymer films processed by solution casting or be served as a protection layer by dip coating. The mechanisms of UV shielding and thermal-oxidative stability are discussed based on effective components such as melanoidin, caffeine, and chlorogenic acid. The work demonstrates yet another route toward fabricating biocompatible and environment-friendly UV-shielding materials with sound overall performance.



INTRODUCTION

Ultraviolet (UV) light generally refers to electromagnetic radiations with wavelength ranging between 10 and 400 nm. It carries high energy and hence is able to break chemical bonds of many organic materials. Therefore, UV irradiation has been widely used in various applications such as sterilization, disinfection, and industrial photoprocessing. On the other hand, it is one of the prime culprits for the degradation and performance loss of polymer-related products, including plastics, paints, and so forth.¹ It can also cause severe injuries to human health by damaging DNA molecules and by suppressing the immune systems, leading to photoaging and carcinogenesis.² Thus, UV-shielding materials have been attracting significant attention not only for scientific and industrial communities but also for the daily life of people. Moreover, it is often advantageous to develop UV-shielding materials that are transparent for visible light, which is of critical importance in applications such as UV-shielding window, contact lens, solar cells and light-emitting diode (LED) encapsulation, food and pharmaceutical packaging, to name just a few.

UV-shielding materials are often produced by incorporating UV filters into matrix materials. Generally, UV filters can be categorized into one of the two classes. Inorganic UV filters include metal oxides such as zinc dioxide (ZnO), titanium

dioxide (TiO₂), and cerium dioxide (CeO₂). They protect materials mainly by reflecting and scattering UV light.³ They can also absorb UV light, and the efficiency is particle-size-dependent.⁴ The other class includes organic UV absorbers such as oxybenzone and octinoxate. These organic compounds often contain conjugate structures, and they absorb UV light and dissipate energy into the environment mainly in the form of heat.⁵ Researchers used to consider inorganic UV filters safer; however, it has been revealed that those oxides can serve as efficient photocatalysts (particularly when the particle size reaches nanometer scale) and can produce highly oxidizing radicals and reactive oxygen species that are cytotoxic and genotoxic, after absorbing UV light.^{6,7} The photocatalytic effect can be mitigated if particle sizes are larger than ~1 μm; however, in this case, the materials are often highly opaque.⁸

Organic UV filters generally have poor biocompatibility. Penetration of these small molecules into epidermal cells and their potential deposition in the adipose tissue have raised

Received: January 23, 2020

Revised: April 2, 2020

Accepted: April 6, 2020

Published: April 24, 2020



substantial concerns.^{9,10} They are also environment unfriendly. For example, a bill banning sunscreens containing oxybenzone and octinoxate has been passed by the Hawaii legislature in 2018 to protect local marine ecosystems, particularly, to prevent coral reef from continuous shrinking.¹¹ More recently, carbon-based fillers (CBFs), particularly graphene family nanomaterials,¹² have attracted much attention for UV-shielding applications. These materials are also prone to produce human and environmental hazard.¹³

With the rising demands of mitigating the damage to the environment and human health, a new generation of UV-shielding materials that are bio-based, biocompatible, and sustainable is much favored. This has been manifested in recent research trend of employing natural materials such as lignin,¹⁴ functionalized cellulose,^{15–19} and melanin nanoparticles,^{20–22} as UV filters. Coffee is a popular beverage, having being consumed for over 1000 years.²³ It stands out as a dietary source of potential antioxidants, including caffeine, chlorogenic acid, and melanoidins.²⁴ Major research has focused on the beneficial effects of coffee on human health.²⁵ As a matter of fact, recently there have been efforts to explore its usefulness in material science. For example, it has been demonstrated that coffee components such as caffeine can be utilized as additives for various applications such as sunscreens and perovskite solar cells.^{26–30}

Considering coffee is abundant in natural polyphenols and antioxidants, we hypothesize that it can also be used as an additive to produce polymer composite with sound UV-shielding performance and thermal stability. In this contribution, we report an attempt to fabricate a transparent UV-shielding composite using coffee extract as the UV filter and poly(vinyl alcohol) (PVA) as the polymer matrix. PVA is selected as the model polymer because it is considered nontoxic and biocompatible. It has good mechanical performance and chemical resistance and has been widely used in textile sizing, coating, adhesive, and film packaging.^{31–34} We demonstrate that coffee can be used to produce polymer materials possessing excellent UV-shielding ability, yet able to maintain a reasonably good visible light transparency. The morphology, UV and thermal stability, and mechanical performances of the obtained PVA/coffee composite are discussed.

EXPERIMENTAL SECTION

Materials. Poly(vinyl alcohol) (PVA) (M_w : 89 000–98 000, >99% hydrolyzed), chlorogenic acid, and caffeine were purchased from Sigma-Aldrich Chemicals. Rhodamine B (GRM 980) was purchased from HIMEDIA. NESCAFE CLASICO dark roast instant coffee (IC) was purchased from a local store. All of the materials were used as received.

Preparation of PVA/IC Composite. PVA/IC composite films were prepared by solution casting. Five percent of PVA solutions (hereafter mass fractions are used for all concentrations) was prepared first. Typically, this is done by adding 1 g of PVA to 20 g of deionized water, keeping the solution stirred at 80 °C for 30 min. IC was then added to the aqueous PVA solutions, and the targeted IC concentrations were 1 and 5%. The solutions were kept stirred for another 10 min and then cast onto Petri dishes and allowed to dry at room temperature. The final film thickness was ≈ 100 μm . Material characterizations were calibrated for thickness variation. PVA/IC composite films with IC concentrations of 1 and 5% were

coded as IC-1 and IC-5, respectively. A pure PVA film without IC was prepared in the same way for comparison purposes.

Material Characterizations. UV–Visible (UV–Vis) Spectroscopy. UV–Vis spectra were recorded in the transmission mode by using a Perkin Elmer Lambda 900 spectrophotometer equipped with an integrating sphere. UV-shielding percentages (S_{UV}) in three different wavelength regions, namely, S_{UVA} for the range between 320 and 400 nm, S_{UVB} between 280 and 320 nm, and S_{UVC} between 200 and 280 nm, are calculated using eqs 1–3

$$S_{UVA} = 1 - T_{UVA} = 1 - \frac{\sum_{320}^{400} T_{\lambda} \times \Delta\lambda}{\sum_{320}^{400} \Delta\lambda} \times 100\% \quad (1)$$

$$S_{UVB} = 1 - T_{UVB} = 1 - \frac{\sum_{280}^{320} T_{\lambda} \times \Delta\lambda}{\sum_{280}^{320} \Delta\lambda} \times 100\% \quad (2)$$

$$S_{UVC} = 1 - T_{UVC} = 1 - \frac{\sum_{200}^{280} T_{\lambda} \times \Delta\lambda}{\sum_{200}^{280} \Delta\lambda} \times 100\% \quad (3)$$

T_{UVA} , T_{UVB} , and T_{UVC} are the averaged transmittance percentage in the three regions, λ and $\Delta\lambda$ are the wavelength and wavelength spread, respectively, and T_{λ} is the spectral transmittance. The averaged transmittance, T_{vis} , in the visible region ranging from 400 to 780 nm of the composite films was calculated by eq 4, which is used to characterize the transparency of the films

$$T_{vis} = \frac{\sum_{400}^{780} T_{\lambda} \times \Delta\lambda}{\sum_{400}^{780} \Delta\lambda} \times 100\% \quad (4)$$

The value of the ultraviolet protection factor (UPF) was also calculated to evaluate the effective protection capability of the PVA/IC composite films against the sunlight by considering its spectral UV damage in terms of erythema.³⁵ UPF is defined as follows

$$UPF = \frac{\sum_{290}^{400} E_{\lambda} \times S_{\lambda} \times \Delta\lambda}{\sum_{290}^{400} E_{\lambda} \times S_{\lambda} \times T_{\lambda} \times \Delta\lambda} \quad (5)$$

where E_{λ} is the solar spectral irradiance, and S_{λ} is the relative erythral spectral effectiveness. Equation 5 is based on parameters measured in the wavelength range between 290 and 400 nm, mimicking the spectrum of natural solar UV irradiation. For aqueous solutions, UV–Vis spectra were collected for liquid samples loaded in quartz cells with 1 mm path length.

UV Shielding of PVA and PVA/IC Composite Films. UV-shielding performance of composite films was first evaluated by monitoring the photodegradation behavior of the rhodamine B. Aqueous rhodamine B solution was loaded into a quartz cell with 5 mm path length and was subjected to the National Institute of Standards and Technology (NIST) simulated photodegradation via high-energy radiant exposure (SPHERE). The NIST SPHERE can provide stable and uniform irradiation in the wavelength range between 290 and 450 nm. Details about specifications of the NIST SPHERE have been reported elsewhere.³⁶ During irradiation, the quartz cell was covered by the testing film (pure PVA or IC-5 composite films). The absorbance ratio, A_r , is defined as

$$A_r = A_t/A_0 \times 100\% \quad (6)$$

where A_0 and A_t are the absorbance of the sample before and after UV irradiation, respectively, which can be used to quantify the degree of photodegradation. Absorbance of rhodamine B solution at 550 nm, which is a well-accepted indicator, is used for calculation of eq 6.

UV stability of the shielding performance of the PVA/IC composite films was evaluated by the accelerated UV aging in the NIST SPHERE for up to 68 h (25 °C, dry condition), with a dose of 40 MJ/m².

UV-shielding capability of the composite films was examined under a UV germicidal lamp (36 W, $\lambda = 254$ nm). Fresh eggplant with the skin areas covered by opaque paper, pure PVA film, and the IC-5 composite film was exposed under the UV germicidal lamp for ≈ 4 h, and the skin color of the eggplant was visually inspected afterward.

Fluorescence and Infrared Thermal Imaging. Fluorescence imaging measurements were carried out by using a Zeiss LSM800 (Carl Zeiss Microscopy, Thornwood, NY) laser scanning confocal microscope with a near-UV excitation wavelength of 405 nm coupled with a long-pass 420 filter. Infrared thermal imaging for the PVA and composite films was performed by employing a thermal camera (Perfect Prime IR0019) under the UV light with a wavelength of 365 nm generated by a 5 W UV LED flashlight with a BLACKOUT filter technology.³⁷

Thermogravimetric Analysis (TGA). TGA measurements were carried out using a TA Q500 thermal analyzer, ramping from 30 to 650 °C with a heating rate of 20 °C/min in an air environment. A constant airflow rate of 50 mL/min was maintained during the measurement.

RESULTS AND DISCUSSIONS

UV Shielding. Roasted coffee contains complex chemicals that depend on the coffee species and roasting procedures. Major components include carbohydrates (24–39%), proteins (13–15%), minerals (3.5–4.5%), and melanoidins (16–17%).³⁸ Among them, coffee melanoidin, a class of high polymer that consisted of a mixture of carbohydrates, amino acids, and phenolic compounds, has been found to have a UV absorption function.³⁹ Other organic compounds, such as chlorogenic acids (1.2–2.3%) and caffeine (1%),³⁸ though small in natural abundance, can also absorb UV light. Figure 1 shows the UV–Vis absorption spectra of the aqueous solution of instant coffee (IC). Two strong peaks are observed in the UV regions. The first absorption band is in the region between 250 and 300 nm, peaked at 280 nm, and the second between

300 and 400 nm, peaked at 325 nm. There is also a broad, weak absorption spreading from 400 to 550 nm, contributing to the slightly brown color. For comparison purposes, the spectra of melanoidin, chlorogenic acids, and caffeine are also shown. Notice that no pure melanoidin standard sample is yet available; the high-molecular-weight coffee fraction is used as the melanoidin standard, which is separated from coffee by using the centrifugal filtration method (10 kDa molecular weight cutoff), following the reported protocol.²⁵ For caffeine, the narrow band peaked at 272 nm is associated with the C=O group.⁴⁰ For chlorogenic acid, the peak at 324 nm with a shoulder around 296 nm can be identified; these bands are due to the highest occupied molecular orbital (HOMO) \rightarrow lowest unoccupied molecular orbital (LUMO) transition with a $\pi \rightarrow \pi^*$ character.⁴¹ Though varied in strength, the absorption spectrum from melanoidin resembles that from IC.^{42–44}

UV-shielding performance of the PVA/IC composite films was evaluated by UV–vis transmittance spectra in the wavelength range between 200 and 800 nm, as shown in Figure 2a. For comparison purposes, the UV–Vis spectrum of pure PVA film was also measured. PVA is known for its excellent optical transparency; seen from Figure 2a, the PVA film shows a high transmittance of 91.5% in the entire visible region (400–800 nm). It is largely transparent to the UVA and UVB light as well: the median values of transmittance are 86.8 and 82.7%, respectively. There is an additional decrease of transmittance of 73.0% in the UVC region from 200 to 280 nm. For PVA/IC composite films, the UV transmittance reduces significantly, whereas the optical transmittance in the visible region is still largely maintained. For example, by introducing only 1% of IC, the UV transmittance (eqs 1–4) of the composite film has already dropped to about 36.1% in UVA, 17.1% in UVB, and 7.4% in UVC region (Figure 2b). When 5% of IC is added, 93, 99.4, and 99.4% of UV lights in the UVA, UVB, and UVC regions are shielded (or equivalently, the transmittance drops to 7, 0.6, and 0.6%, respectively), while the transparency in the visible region can still maintain at a level of 77%. A visual check of PVA/IC composite films with different IC contents on top of a text background is shown in Figure 2c. IC-1 film is largely clear. For IC-5 film, though a light brown color shows up, the texts underneath are clearly visible. UPFs (eq 5) are used to evaluate the protection capability of the composite film against the sun. UPF was classified into three categories according to the latest AS/NZS 4399:2017 standard:³⁵ minimum (UPF > 15), good protection (UPF > 30), and excellent protection (UPF > 50, 50+). UPF of the IC-5 film exceeds 80, which falls in the grade of excellent UV protection.

Comparison of the overall performance of different transparent UV-shielding materials is carried out by employing Ashby plots, as shown in Figure 2d. The percentages of transparency and shielding at given wavelengths are represented in x - and y -axes, respectively, in an Ashby plot. In Figure 2d, the visible transparency of the materials is characterized by the transmittance at the wavelength of 550 nm, and the UV-shielding ability is characterized by the absorptivity at 300 nm (UVB region) and 350 nm (UVA region). Wavelengths of 300 and 350 nm were selected because the most damaging natural UV radiation is between 290 and 350 nm; they are also widely used in the literature.^{45,46} The blue arrows in the Ashby plots show the trend that a material can simultaneously possess good visible transparency and UV-shielding performance. Data points located in the right

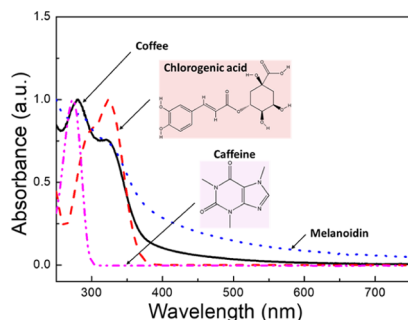


Figure 1. UV–Vis absorbance spectra of the aqueous solutions (0.05 mg/mL) of instant coffee, chlorogenic acid, caffeine, and melanoidin. Spectra are normalized to their maximum absorbance. Chemical structures of chlorogenic acid and caffeine are shown in the insets.

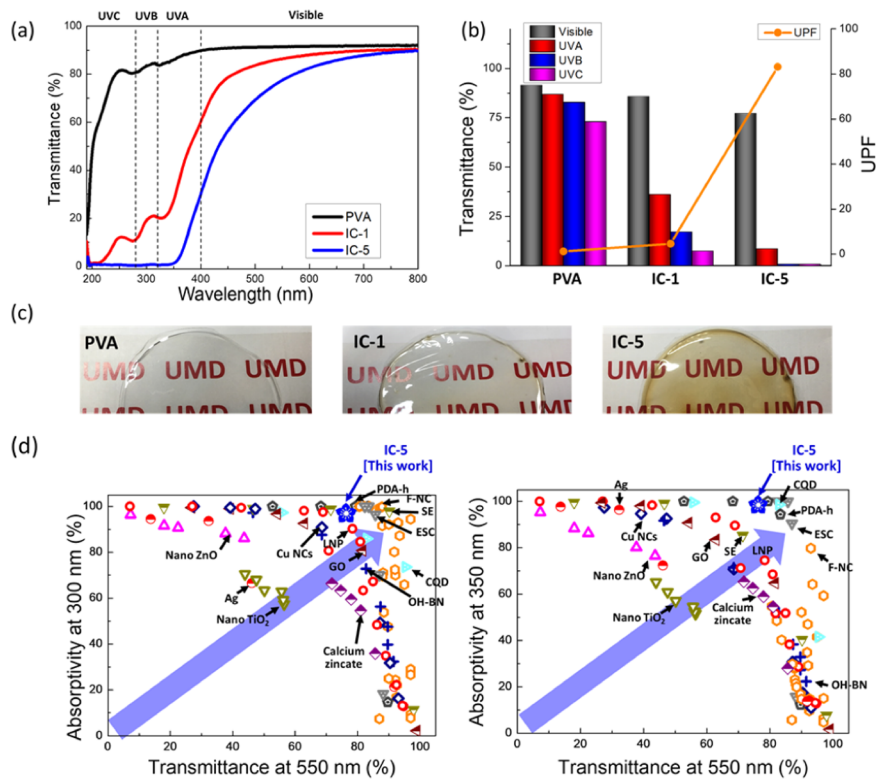


Figure 2. (a) UV–Vis transmittance curves of pure PVA, IC-1, and IC-5 films; (b) corresponding bar chart of the transmittance at the UVA, UVB, and UVC regions, and the protection factor (UPF); (c) visual comparison of the three films; (d) comparison of the overall performance (Ashby plot using the absorptivity at 300 and 350 nm and the transmittance at 550 nm) of the IC-5 film and that of the reported materials (LNP: lignin nanospheres,¹⁴ PDA-h: polydopamine hollow nanoparticles,²¹ F-NC: functionalized nanocellulose,^{16,19,47,48} SE: sepia eumelanin,²⁰ ESC: esculetin,⁴⁹ nano-ZnO,⁵⁰ Cu Ncs: copper nanocluster,⁵¹ GO: graphene oxide,¹² Ag: Ag nanoparticle,⁵² CQD: carbon quantum dot,⁴⁶ OH-BN: hydroxylated boron nitride,⁵³ nano-TiO₂,⁵⁴ calcium zincate⁵⁵).

corner of the plots correspond to the materials having the best-combined properties. Data from reported materials such as lignin nanospheres, polydopamine nanoparticles, and functionalized nanocellulose are reported values.^{14,16,19,21,47,48} Seen from Figure 2d, the IC-5 film possesses an excellent overall transparent UV-shielding performance over the full spectrum.

Note that PVA is a semicrystalline polymer. As revealed by differential scanning calorimetry (DSC), the solution-cast pure PVA has a crystallinity of 32.2% and a melting point of 227.6 °C (see Figure S1 in the Supporting Information). Adding IC can slightly increase the crystallinity and the melting temperature. For the IC-5 sample, the crystallinity and the melting temperature are increased to 37.2 and 228.4 °C, respectively (Figure S1), which could be attributed to the effect of nucleation. In general, higher crystallinity and larger crystal size are prone to increase the turbidity of a material. However, this effect should be minor in the PVA/IC composite, as the absorption of visible light is dictated by the coloring effect due to the addition of IC, as seen in Figure 2.

The absorbance ratio A_t of rhodamine B (eq 6) is used to evaluate the UV-shielding efficiency of the IC-5 composite film. Figure 3 shows the change of A_t as a function of time for rhodamine B shielded with the IC-5 film. The exposure test was carried out in the NIST SPHERE. In the linear plot as shown in Figure 3a, A_t decreases quickly in the first 2 h, followed by a slow decay in the rest of the time of the experiment. The linear relationship as seen from the $-\ln A_t$ versus time plot in Figure 3b suggests a photodegradation

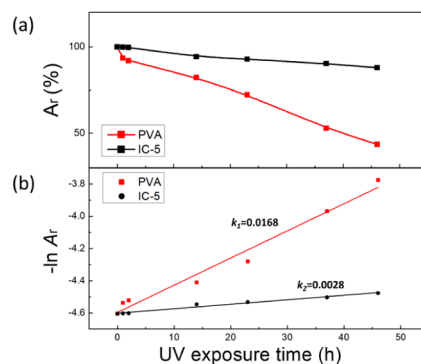


Figure 3. Change of the absorbance ratio A_t of the rhodamine B solutions shielded by pure PVA and the IC-5 composite films as a function of UV exposure time (a), and the corresponding $-\ln(A_t)$ versus time plot in which the slopes (k_1 and k_2) characterize the photodegradation rates (b).

process following the pseudo-first-order kinetic model.^{56,57} Photodegradation rates can be obtained from the slopes of the decay functions; they are 0.0168 and 0.0028 h⁻¹ for rhodamine B shielded by pure PVA and IC-5 composite films, respectively. In other words, the UV-shielding efficiency of the IC-5 film is about 6 times higher, compared with that of the pure PVA film. It can be estimated that, after converting the UV dose of the NIST SPHERE simulator to that of the natural environment, the protection from PVA/IC composites can extend the lifetime of UV-sensitive materials from days to weeks.

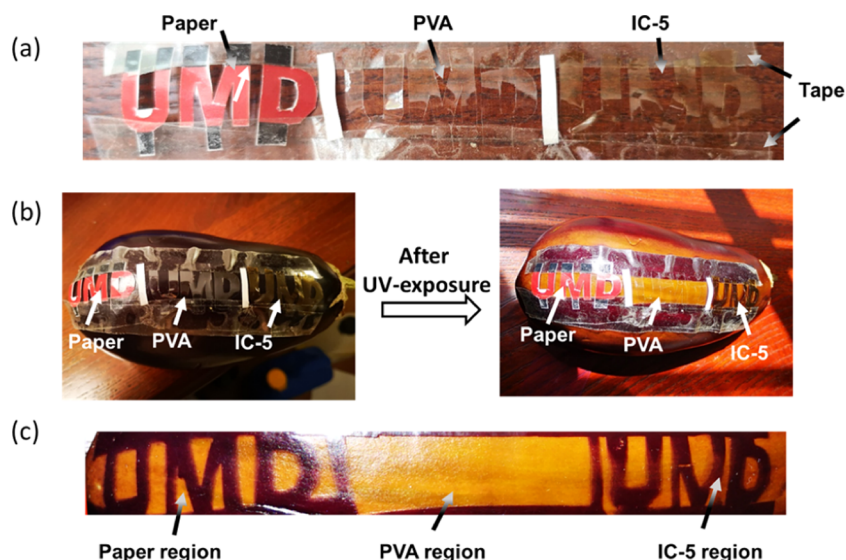


Figure 4. Demonstration of photoprotection against UV light for the eggplant peel using IC-5 composite film: (a) masking scheme using paper, pure PVA film, and the IC-5 film; (b) masked eggplant before and after UV exposure; and (c) zoom-in view of the masked regions after UV exposure.

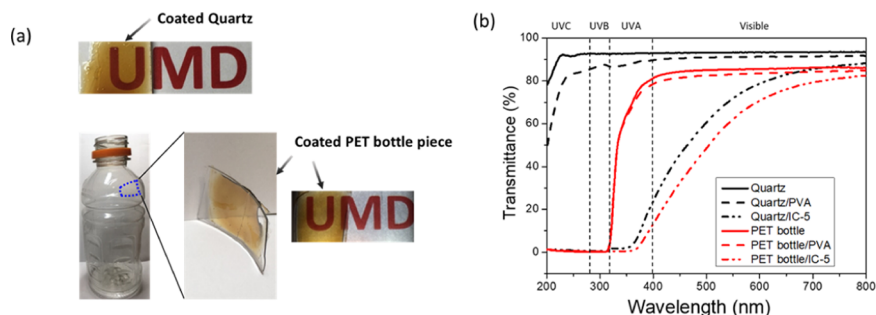


Figure 5. (a) Images for quartz slide and PET bottle piece dip-coated with the IC-5 and (b) UV–Vis transmittance curves for quartz slide and PET bottle piece with and without a coating layer.

High UV-shielding efficiency and high visible light transparency together with good biocompatibility make the PVA/IC composite film potentially useful in applications such as food packaging. As a demonstration, the protection of eggplant from UV damage by covering it with a PVA/IC film is shown in Figure 4. Anthocyanins existing in the peel of fruits such as eggplant and red radish are one of the major categories of natural pigments. They have been used as industrial colorants, food colorants and supplements, PH indicator, etc.⁵⁸ However, they are prone to degrade when being subjected to UV exposure.⁵⁹ In Figure 4, the eggplant protected by opaque paper (red in color), transparent PVA film, and the IC-5 film (Figure 4a,b) was subjected to a UV germicidal lamp with a wavelength spread peaked at 254 nm. After 4 h of exposure, obvious photofading in the uncovered region, as well as the PVA-film-covered region, is evident (Figure 4b,c), while the color in the regions covered by the IC-5 film remains almost unchanged. Moreover, the addition of IC extract to PVA does not significantly influence the mechanical properties of the materials (see Figure S2 in the Supporting Information).

Besides making films, PVA/IC composites can also be used as coating materials. Figure 5a shows a quartz slide and clear poly(ethylene terephthalate) (PET) bottle dip-coated with IC-5. To obtain an approximately 100 μm coating layer, 15% of IC-5 solution was prepared, and the substrates (quartz slide or

a bottle piece) were dipped in the solution, followed by drying at 40 °C in a vacuum oven until no mass loss was observed. The coated quartz and PET bottle piece can still maintain a certain degree of visible transparency, as seen in Figure 5a. The corresponding UV transmittance spectra are shown in Figure 5b. For the coated samples, about 90% of UV light has been shielded, while the transparency in the visible region above 550 nm is higher than 60%. Notice that PET polymer itself has strong UV absorption in the UVB and UVC regions (<320 nm) due to the existence of aromatic rings in the polymer chain backbones, but it is largely transparent in the UVA region. PVA/IC coating can provide essential UV shielding in the UVA range, which is potentially useful in preventing damage due to sunlight. One should be reminded that, although the shorter-wavelength and higher-energy UVB light in sunlight has relatively higher efficiency in causing degradation, UVA light also plays an important role in certain photodegradation reactions,^{60,61} due to its dominance in percentage.

UV Stability. UV stability is another critical property that has an influence on the long-term service of materials. The IC-5 film was exposed to UV light in the NIST SPHERE, which provided stable and uniform irradiation ranging from 290 to 550 nm with the UV irradiance (between 300 and 400 nm) of about 170 W/m^2 . The UV radiation (40 MJ/m^2 for 68 h) is

approximately equivalent to that caused by a 45-day exposure in Miami, Florida, where the annual average UV dose is 320 MJ/m².⁶² Figure 6 shows transmittance curves of the IC-5 film

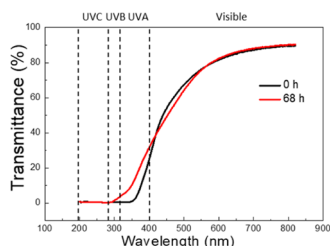


Figure 6. UV–Vis transmittance curves of the IC-5 composite film before (0 h) and after (40 MJ/m² for 68 h) accelerated UV aging.

before and after accelerated UV aging. The major change takes place in the UVA region, where the UV-shielding percentage of the aged IC-5 film, S_{UVA} , dropped from 93 to 84% (eq 1). This might be caused by the degradation of natural UV filters in the IC.⁶³ There is also a less than 1% decrease of transmittance in the visible light region between 420 and 550 nm. Overall, the IC-5 composite film is stable during the UV irradiation.

Energy dissipation pathway of the PVA/IC composite after absorbing UV light is discussed. Generally speaking, UV filter molecules are excited from their ground-state S_0 to a higher-energy electronic-state S_1 after absorbing UV light, as schematically shown in Figure 7a. S_1 state is unstable and is potentially reactive. The stability of a UV filter is largely determined by how the excited molecules can return to its original state. Thus, a reliable UV absorber requires not only absorbing UV light but also the ability to efficiently dissipate the absorbed energy in a harmless way, i.e., lowering its energy without producing free radicals or other hazardous photo-degradation species. In this regard, energy dissipation via physical pathways, such as via fluorescence or heat transfer (to the environment), is preferred. It has been found that both the mechanisms work for the PVA/IC composite.

The first pathway is via the fluorescence emission. Fluorescence images of the IC-5 film, PVA contained 5% of chlorogenic acid (CGA-5), and melanoidin (MD-5), excited by near-UV light with a wavelength of 405 nm, are shown in Figure 7b. No fluorescence is observed for pure PVA film, while a blue-green fluorescence is evident for the IC-5 film; the fluorescence spectrum shows a maximum at around 525 nm. Similar fluorescence spectra are observed for the CGA-5 and

MD-5 samples, suggesting that they might be the effective components in IC responsible for the fluorescence emission.

To verify whether heat dissipation serves as another mechanism, infrared thermal imaging of the IC-5 film was conducted; the results are shown in Figure 7c. Under UV irradiation with a wavelength of 365 nm, the maximum temperature is 29 °C for the pure PVA film, while it increases to 34.4 °C for the IC-5 film. Energy from the excited state could be dissipated through direct radiationless deactivation, intersystem crossing, ring-centered out-of-plane deformations, tautomerization, etc.,^{5,64} which might cause the increase of temperature in the radiated area. Similar heat dissipation effects are also observed for CGA-5 (32.5 °C) and MD-5 (33.0 °C) composite films.

Thermal-Oxidative Stability. Thermal-oxidative stability of the PVC/IC composite was tested by using thermal gravimetric analysis (TGA) in an air environment. Figure 8

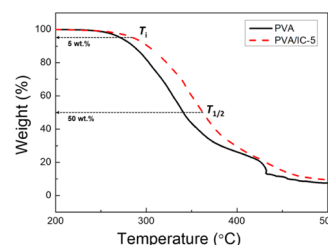


Figure 8. TGA curves of pure PVA and the IC-5 composite films under an air atmosphere at a heating rate of 20 °C/min. T_i and $T_{1/2}$ are defined as the temperatures at which mass loss reaches 5% and 50%, respectively.

shows the TGA traces of pure PVA and the IC-5 composite films in the temperature range between 200 and 500 °C. Weight loss of the pure PVA film starts at ≈ 250 °C. Thermal degradation mechanism of PVA polymer has been well studied. Since we used PVA with a high hydrolysis level (>99%), the hydroxyl group is the major functional group on the chain backbone. During thermal degradation, the decomposed hydroxyl radicals can attack hydrogen on the backbone to form new free radicals and cause dehydration,^{65–67} and the reaction propagates in an accelerating manner. The temperatures at which the weight loss reaches 5 and 50%, denoted as T_i and $T_{1/2}$, are used to parameterize the thermal-oxidative stability.⁴⁹ Seen from Figure 8, for pure PVA, T_i and $T_{1/2}$ are 271 and 341 °C, respectively. Addition of 5% of IC results in an increase of T_i and $T_{1/2}$ by 15 °C and 22 °C, respectively.

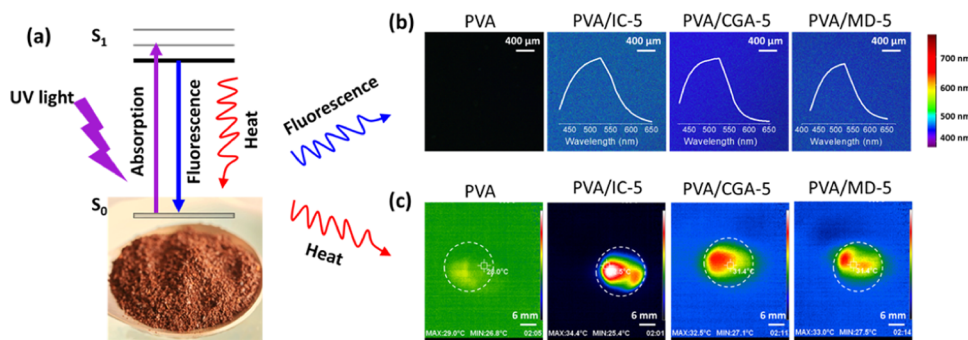


Figure 7. Scheme of UV absorption and energy release (a), fluorescence images and spectra (b), and infrared thermal images (sample areas are circled) (c) of pure PVA film and composite films of IC-5, chlorogenic acid (5%, CGA-5), and melanoidin (5%, MD-5).

The increase of the thermal stability of the PVA/IC composite might be due to two reasons. First, chemicals in IC, such as caffeine, chlorogenic acid, and melanoidin, can effectively serve as radical scavengers and can react with the free radicals formed during degradation, which delays the elimination of hydroxyl groups. Antioxidant effect of coffee has been well applied in nutrition sciences.^{24,68–70} For example, roasted coffee has been shown to be able to effectively slow down the oxidation processes and has been used as an additive to extend the shelf life of food products.⁶⁹ There is also evidence showing that the consumption of coffee brew can reduce the oxidative damage of DNA molecules and can increase their tolerance against oxidants.⁷⁰ Second, chemicals in IC contain a rich amount of functional groups that are readily served as electron donors and can form hydrogen bonds with the hydroxyl groups on PVA backbones. Hydrogen bonding between antioxidant with the polymer has been reported. A fingerprint of this effect is observed in FTIR spectra: the 3274 cm^{-1} peak due to the stretching of the hydroxyl group is slightly blue-shifted to 3283 cm^{-1} (see Figure S3a in the Supporting Information). Formation of hydrogen bonding between PVA and IC can also cause a slowdown of PVA chain dynamics and hence retard the propagation of the oxidation process.^{66,71,72} It has been observed that with an increase of the IC content, the glass-transition temperature of the IC-5 composite slightly increases (see Figure S3b in the Supporting Information), which provides indirect evidence of the slowdown of the dynamics. A comprehensive discussion of the antioxidation mechanism is subject to future studies.

CONCLUSIONS

Polymer composite with sound UV-shielding property and visible light transparency was produced by hybridizing instant coffee (IC) with the PVA matrix. Addition of 5% of IC into PVA polymer effectively shielded over 93, 99.4, and 99.4% of UV light in the UVA, UVB, and UVC regions respectively; more than 77% of transparency was retained in the visible region. The UV-shielding ability was largely maintained under the accelerated aging condition with a UV dose of 40 MJ/m^2 for 68 h. Moreover, the thermal-oxidative stability of the PVA/IC composite was also improved, with an increase in the onset decomposition temperature T_i of ≈ 15 $^{\circ}\text{C}$ and the temperature of 50% mass loss $T_{1/2}$ of ≈ 22 $^{\circ}\text{C}$. The overall performance of the composite might be due to the effective components such as melanoidin, caffeine, and chlorogenic acid in IC. For UV shielding and UV stability, the absorbed UV energy was dissipated via the routes of both fluorescence emission and photothermal conversion. The thermal-oxidative stability was mostly attributed to the antioxidation function of the effective components; the specific interaction between the small molecules and PVA polymer might also play a role.

ASSOCIATED CONTENT

Supporting Information

The Supporting Information is available free of charge at <https://pubs.acs.org/doi/10.1021/acs.iecr.0c00413>.

DSC melting traces of PVA and PVA/IC-5 composite (Figure S1); typical stress–strain curves for pure PVA and IC-5 composite films (Figure S2); and FTIR spectra and DSC curves of pure PVA and IC-5 composite films (Figure S3) (PDF)

AUTHOR INFORMATION

Corresponding Authors

Xiaohong Gu – Engineering Laboratory, National Institute of Standards and Technology, Gaithersburg, Maryland 20899, United States; Phone: +1 301 975 6523;

Email: xiaohong.gu@nist.gov

Yimin Mao – Department of Materials Science and Engineering, University of Maryland, College Park, Maryland 20742, United States; NIST Center for Neutron Research, National Institute of Standards and Technology, Gaithersburg, Maryland 20899, United States; orcid.org/0000-0002-6240-3791; Phone: +1 301 975 6017; Email: yimin.mao@nist.gov

Author

Yadong Lyu – Engineering Laboratory, National Institute of Standards and Technology, Gaithersburg, Maryland 20899, United States

Complete contact information is available at:

<https://pubs.acs.org/10.1021/acs.iecr.0c00413>

Notes

Certain commercial products or equipment are described in this paper to specify adequately the experimental procedure. In no case does such identification imply recommendation or endorsement by the National Institute of Standards and Technology, nor does it imply that it is necessarily the best available for the purpose.

The authors declare no competing financial interest.

ACKNOWLEDGMENTS

This work was partially supported under the NIST cooperative agreement 70NANB15H261.

REFERENCES

- (1) McKeen, L. W. *The effect of UV Light and Weather on Plastics and Elastomers*. William Andrew, Inc., 2019.
- (2) Maverakis, E.; Miyamura, Y.; Bowen, M. P.; Correa, G.; Ono, Y.; Goodarzi, H. Light, including ultraviolet. *J. Autoimmun.* **2010**, *34*, J247–J257.
- (3) Cole, C.; Shyr, T.; Ou-Yang, H. Metal oxide sunscreens protect skin by absorption, not by reflection or scattering. *Photodermatol., Photoimmunol. Photomed.* **2016**, *32*, 5–10.
- (4) Popov, A.; Priezzhev, A.; Lademann, J.; Myllylä, R. TiO₂ nanoparticles as an effective UV-B radiation skin-protective compound in sunscreens. *J. Phys. D: Appl. Phys.* **2005**, *38*, 2564.
- (5) Karsili, T. N.; Marchetti, B.; Ashfold, M. N.; Domcke, W. Ab initio study of potential ultrafast internal conversion routes in oxybenzone, caffeic acid, and ferulic acid: Implications for sunscreens. *J. Phys. Chem. A* **2014**, *118*, 11999–12010.
- (6) Zhang, Z.; Wang, C.-C.; Zakaria, R.; Ying, J. Y. Role of particle size in nanocrystalline TiO₂-based photocatalysts. *J. Phys. Chem. B* **1998**, *102*, 10871–10878.
- (7) Dodd, A.; McKinley, A.; Saunders, M.; Tsuzuki, T. Effect of particle size on the photocatalytic activity of nanoparticulate zinc oxide. *J. Nanopart. Res.* **2006**, *8*, 43.
- (8) Schneider, S. L.; Lim, H. W. A review of inorganic UV filters zinc oxide and titanium dioxide. *Photodermatol., Photoimmunol. Photomed.* **2018**, *35*, 1–5.
- (9) Hayden, C.; Cross, S.; Anderson, C.; Saunders, N.; Roberts, M. Sunscreen penetration of human skin and related keratinocyte toxicity after topical application. *Skin Pharmacol. Physiol.* **2005**, *18*, 170–174.
- (10) Matta, M. K.; Zusterzeel, R.; Pilli, N. R.; Patel, V.; Volpe, D. A.; Florian, J.; Oh, L.; Bashaw, E.; Zineh, I.; Sanabria, C. Effect of sunscreen application under maximal use conditions on plasma

concentration of sunscreen active ingredients: a randomized clinical trial. *JAMA* **2019**, *321*, 2082–2091.

(11) SB2571, https://www.capitol.hawaii.gov/session2018/bills/SB2571_HTM. 2018 (accessed Oct 2019).

(12) Xie, S.; Zhao, J.; Zhang, B.; Wang, Z.; Ma, H.; Yu, C.; Yu, M.; Li, L.; Li, J. Graphene oxide transparent hybrid film and its ultraviolet shielding property. *ACS Appl. Mater. Interfaces* **2015**, *7*, 17558–17564.

(13) Fadeel, B.; Bussy, C.; Merino, S.; Vázquez, E.; Flahaut, E.; Mouchet, F.; Evariste, L.; Gauthier, L.; Koivisto, A. J.; Vogel, U.; et al. Safety assessment of graphene-based materials: focus on human health and the environment. *ACS Nano* **2018**, *12*, 10582–10620.

(14) Xiong, F.; Wu, Y.; Li, G.; Han, Y.; Chu, F. Transparent nanocomposite films of lignin nanospheres and poly (vinyl alcohol) for UV-absorbing. *Ind. Eng. Chem. Res.* **2018**, *57*, 1207–1212.

(15) Zhang, Z.; Sèbe, G.; Wang, X.; Tam, K. C. UV-absorbing cellulose nanocrystals as functional reinforcing fillers in poly (vinyl chloride) films. *ACS Appl. Nano Mater.* **2018**, *1*, 632–641.

(16) Sirviö, J. A.; Visanko, M.; Heiskanen, J. P.; Liimatainen, H. UV-absorbing cellulose nanocrystals as functional reinforcing fillers in polymer nanocomposite films. *J. Mater. Chem. A* **2016**, *4*, 6368–6375.

(17) Abdalkarim, S. Y. H.; Yu, H.-Y.; Wang, C.; Yang, L.; Guan, Y.; Huang, L.; Yao, J. Sheet-like cellulose nanocrystal-ZnO nanohybrids as multifunctional reinforcing agents in biopolyester composite nanofibers with ultrahigh UV-Shielding and antibacterial performances. *ACS Appl. Biol. Mater.* **2018**, *1*, 714–727.

(18) Cazón, P.; Vázquez, M.; Velazquez, G. Composite Films with UV-Barrier Properties Based on Bacterial Cellulose Combined with Chitosan and Poly (vinyl alcohol): Study of Puncture and Water Interaction Properties. *Biomacromolecules* **2019**, *20*, 2084–2095.

(19) Zhang, Z.; Zhang, B.; Grishkewich, N.; Berry, R.; Tam, K. C. Cinnamate-Functionalized Cellulose Nanocrystals as UV-Shielding Nanofillers in Sunscreen and Transparent Polymer Films. *Adv. Sustainable Syst.* **2019**, *3*, No. 1800156.

(20) Wang, Y.; Li, T.; Ma, P.; Bai, H.; Xie, Y.; Chen, M.; Dong, W. Simultaneous enhancements of UV-shielding properties and photostability of poly (vinyl alcohol) via incorporation of sepia eumelanin. *ACS Sustainable Chem. Eng.* **2016**, *4*, 2252–2258.

(21) Wang, Y.; Su, J.; Li, T.; Ma, P.; Bai, H.; Xie, Y.; Chen, M.; Dong, W. A novel UV-shielding and transparent polymer film: when bioinspired dopamine–melanin hollow nanoparticles join polymers. *ACS Appl. Mater. Interfaces* **2017**, *9*, 36281–36289.

(22) Wang, C.; Wang, D.; Dai, T.; Xu, P.; Wu, P.; Zou, Y.; Yang, P.; Hu, J.; Li, Y.; Cheng, Y. Skin Pigmentation-Inspired Polydopamine Sunscreens. *Adv. Funct. Mater.* **2018**, *28*, No. 1802127.

(23) Mussatto, S. I.; Machado, E. M.; Martins, S.; Teixeira, J. A. Production, composition, and application of coffee and its industrial residues. *Food Bioprocess Technol.* **2011**, *4*, 661.

(24) Vignoli, J.; Bassoli, D.; Benassi, M. Antioxidant activity, polyphenols, caffeine and melanoidins in soluble coffee: The influence of processing conditions and raw material. *Food Chem.* **2011**, *124*, 863–868.

(25) Ciaramelli, C.; Palmioli, A.; Airolidi, C. Coffee variety, origin and extraction procedure: Implications for coffee beneficial effects on human health. *Food Chem.* **2019**, *278*, 47–55.

(26) Rosado, C.; Tokunaga, V. K.; Sauce, R.; de Oliveira, C. A.; Sarruf, F. D.; Parise-Filho, R.; Mauricio, E.; de Almeida, T. S.; Velasco, M. V. R.; Baby, A. R. Another Reason for Using Caffeine in Dermocosmetics: Sunscreen Adjuvant. *Front. Physiol.* **2019**, *10*, 1–8.

(27) Cho, Y.-H.; Bahuguna, A.; Kim, H.-H.; Kim, D.-i.; Kim, H.-J.; Yu, J.-M.; Jung, H.-G.; Jang, J.-Y.; Kwak, J.-H.; Park, G.-H. Potential effect of compounds isolated from *Coffea arabica* against UV-B induced skin damage by protecting fibroblast cells. *J. Photochem. Photobiol. B* **2017**, *174*, 323–332.

(28) Rivelli, D. P.; Filho, C. A.; Almeida, R. L.; Ropke, C. D.; Sawada, T. C.; Barros, S. B. Chlorogenic acid UVA–UVB photostability. *Photochem. Photobiol.* **2010**, *86*, 1005–1007.

(29) Kawasumi, M.; Lemos, B.; Bradner, J. E.; Thibodeau, R.; Kim, Y.-s.; Schmidt, M.; Higgins, E.; Koo, S.-w.; Angle-Zahn, A.; Chen, A.

et al. Protection from UV-induced skin carcinogenesis by genetic inhibition of the ataxia telangiectasia and Rad3-related (ATR) kinase. *Proc. Natl. Acad. Sci. U.S.A.* **2011**, *108*, 13716–13721.

(30) Wang, R.; Xue, J.; Meng, L.; Lee, J.-W.; Zhao, Z.; Sun, P.; Cai, L.; Huang, T.; Wang, Z.; Wang, Z.-K.; et al. Caffeine Improves the Performance and Thermal Stability of Perovskite Solar Cells. *Joule* **2019**, *3*, 1464–1477.

(31) Halima, N. B. Poly (vinyl alcohol): review of its promising applications and insights into biodegradation. *RSC Adv.* **2016**, *6*, 39823–39832.

(32) De, S.; Lutkenhaus, J. L. Corrosion behaviour of eco-friendly airbrushed reduced graphene oxide-poly (vinyl alcohol) coatings. *Green Chem.* **2018**, *20*, 506–514.

(33) Hunt, A. J.; Budarin, V. L.; Breeden, S. W.; Matharu, A. S.; Clark, J. H. Expanding the potential for waste polyvinyl-alcohol. *Green Chem.* **2009**, *11*, 1332–1336.

(34) Gonzalez-Ortiz, D.; Pochat-Bohatier, C.; Gassara, S.; Cambedouzou, J.; Bechelany, M.; Miele, P. Development of novel h-BNNS/PVA porous membranes via Pickering emulsion templating. *Green Chem.* **2018**, *20*, 4319–4329.

(35) *Sun Protective Clothing—Evaluation and Classification*. AS/NZS 4399:2017, Standards Australia.

(36) Chin, J.; Byrd, E.; Embree, N.; Garver, J.; Dickens, B.; Finn, T.; Martin, J. Accelerated UV weathering device based on integrating sphere technology. *Rev. Sci. Instrum.* **2004**, *75*, 4951–4959.

(37) https://www.waveformlighting.com/photometrics/TR_7010.365.pdf (accessed on Dec 2019).

(38) Bekedam, E. K. *Coffe Brew Melanoidins. Structural and Functional Properties of Brown-Colored Coffee Compounds*; Wageningen University, 2008.

(39) Rufián-Henares, J. A.; Pastoriza, S. Melanoidins in Coffee, In *Coffee in Health and Disease Prevention*, Preedy, V. R., Ed.; Elsevier, 2015.

(40) Navarra, G.; Moschetti, M.; Guarrasi, V.; Mangione, M.; Militello, V.; Leone, M. Simultaneous determination of caffeine and chlorogenic acids in green coffee by UV/Vis spectroscopy. *J. Chem.* **2017**, *2017*, 1–8.

(41) Cornard, J.-P.; Lapouge, C.; Dangleterre, L.; Allet-Bodelot, C. Complexation of lead (II) by chlorogenic acid: experimental and theoretical study. *J. Phys. Chem. A* **2008**, *112*, 12475–12484.

(42) Borrelli, R. C.; Visconti, A.; Mennella, C.; Anese, M.; Fogliano, V. Chemical characterization and antioxidant properties of coffee melanoidins. *J. Agric. Food Chem.* **2002**, *50*, 6527–6533.

(43) Belay, A.; Gholap, A. Characterization and determination of chlorogenic acids (CGA) in coffee beans by UV-Vis spectroscopy. *Afr. J. Pure Appl. Chem.* **2009**, *3*, 34–240.

(44) Belay, A.; Ture, K.; Redi, M.; Asfaw, A. Measurement of caffeine in coffee beans with UV/vis spectrometer. *Food Chem.* **2008**, *108*, 310–315.

(45) Cui, H.; Zayat, M.; Parejo, P. G.; Levy, D. Highly Efficient Inorganic Transparent UV-Protective Thin-Film Coating by Low Temperature Sol-Gel Procedure for Application on Heat-Sensitive Substrates. *Adv. Mater.* **2008**, *20*, 65–68.

(46) Hess, S. C.; Permatasari, F. A.; Fukazawa, H.; Schneider, E. M.; Balgis, R.; Ogi, T.; Okuyama, K.; Stark, W. J. Direct synthesis of carbon quantum dots in aqueous polymer solution: one-pot reaction and preparation of transparent UV-blocking films. *J. Mater. Chem. A* **2017**, *5*, 5187–5194.

(47) Niu, X.; Liu, Y.; Fang, G.; Huang, C.; Rojas, O. J.; Pan, H. Highly Transparent, Strong, and Flexible Films with Modified Cellulose Nanofiber Bearing UV Shielding Property. *Biomacromolecules* **2018**, *19*, 4565–4575.

(48) Sirviö, J. A.; Visanko, M. Highly Transparent Nanocomposites Based on Poly (vinyl alcohol) and Sulfated UV-Absorbing Wood Nanofibers. *Biomacromolecules* **2019**, *20*, 2413–2420.

(49) Wang, Y.; Xiang, C.; Li, T.; Ma, P.; Bai, H.; Xie, Y.; Chen, M.; Dong, W. Enhanced thermal stability and UV-shielding properties of poly (vinyl alcohol) based on Esculetin. *J. Phys. Chem. B* **2017**, *121*, 1148–1157.

- (50) Liu, X.; Chen, X.; Ren, J.; Chang, M.; He, B.; Zhang, C. Effects of nano-ZnO and nano-SiO₂ particles on properties of PVA/xylan composite films. *Int. J. Biol. Macromol.* **2019**, *132*, 978–986.
- (51) Shi, Ye.; Zhuang, X.; Cao, L.; Gou, S.; Xiong, Y.; Lai, W. F.; Wang, Z.; Rogach, A. L. Copper-Nanocluster-Based Transparent Ultraviolet-Shielding Polymer Films. *ChemNanoMat* **2019**, *5*, 110–115.
- (52) Chahal, R. P.; Mahendia, S.; Tomar, A.; Kumar, S. SHI irradiated PVA/Ag nanocomposites and possibility of UV blocking. *Opt. Mater.* **2016**, *52*, 237–241.
- (53) Cai, W.; Zhang, D.; Wang, B.; Shi, Y.; Pan, Y.; Wang, J.; Hu, W.; Hu, Y. Scalable one-step synthesis of hydroxylated boron nitride nanosheets for obtaining multifunctional polyvinyl alcohol nanocomposite films: Multi-azimuth properties improvement. *Compos. Sci. Technol.* **2018**, *168*, 74–80.
- (54) Kochkina, N. E.; Butikova, O. A. Effect of fibrous TiO₂ filler on the structural, mechanical, barrier and optical characteristics of biodegradable maize starch/PVA composite films. *Int. J. Biol. Macromol.* **2019**, *139*, 431–439.
- (55) Subramani, N. K.; Kasargod Nagaraj, S.; Shivanna, S.; Siddaramaiah, H. Highly flexible and visibly transparent poly (vinyl alcohol)/calcium zincate nanocomposite films for UVA shielding applications as assessed by novel ultraviolet photon induced fluorescence quenching. *Macromolecules* **2016**, *49*, 2791–2801.
- (56) Wilhelm, P.; Stephan, D. Photodegradation of rhodamine B in aqueous solution via SiO₂@ TiO₂ nano-spheres. *J. Photochem. Photobiol. A* **2007**, *185*, 19–25.
- (57) Wang, Z.; Chen, C.; Wu, F.; Zou, B.; Zhao, M.; Wang, J.; Feng, C. Photodegradation of rhodamine B under visible light by bimetal codoped TiO₂ nanocrystals. *J. Hazard. Mater.* **2009**, *164*, 615–620.
- (58) Silva, S.; Costa, E.; Calhau, C.; Morais, R.; Pintado, M. Anthocyanin extraction from plant tissues: A review. *Crit. Rev. Food Sci. Nutr.* **2017**, *57*, 3072–3083.
- (59) Bąkowska, A.; Kucharska, A. Z.; Oszmiański, J. The effects of heating, UV irradiation, and storage on stability of the anthocyanin–polyphenol copigment complex. *Food Chem.* **2003**, *81*, 349–355.
- (60) Therias, S.; Dintcheva, N. T.; Gardette, J.-L.; La Mantia, F. P. Photooxidative behaviour of polyethylene/polyamide-6 blends. *Polym. Degrad. Stab.* **2010**, *95*, 522–526.
- (61) Andrady, A. L.; Searle, N. D.; Crewdson, L. F. Wavelength sensitivity of unstabilized and UV stabilized polycarbonate to solar simulated radiation. *Polym. Degrad. Stab.* **1992**, *35*, 235–247.
- (62) <http://www.atlaswsg.com/weath/2007.pdf> (accessed Dec 2019).
- (63) Karaköse, H.; Jaiswal, R.; Deshpande, S.; Kuhnert, N. Investigation of the photochemical changes of chlorogenic acids induced by ultraviolet light in model systems and in agricultural practice with *Stevia rebaudiana* cultivation as an example. *J. Agric. Food Chem.* **2015**, *63*, 3338–3347.
- (64) Kinoshita, S.-n.; Miyazaki, Y.; Sumida, M.; Onitsuka, Y.; Kohguchi, H.; Inokuchi, Y.; Akai, N.; Shiraogawa, T.; Ehara, M.; Yamazaki, K. Different photoisomerization routes found in the structural isomers of hydroxy methylcinnamate. *Phys. Chem. Chem. Phys.* **2018**, *20*, 17583–17598.
- (65) Wang, D.-L.; Liu, Y.; Wang, D.-Y.; Zhao, C.-X.; Mou, Y.-R.; Wang, Y.-Z. A novel intumescent flame-retardant system containing metal chelates for polyvinyl alcohol. *Polym. Degrad. Stab.* **2007**, *92*, 1555–1564.
- (66) Song, Pa.; Xu, Z.; Lu, Y.; Guo, Q. Bioinspired strategy for tuning thermal stability of PVA via hydrogen-bond crosslink. *Compos. Sci. Technol.* **2015**, *118*, 16–22.
- (67) Dong, W.; Wang, Y.; Huang, C.; Xiang, S.; Ma, P.; Ni, Z.; Chen, M. Enhanced thermal stability of poly (vinyl alcohol) in presence of melanin. *J. Therm. Anal. Calorim.* **2014**, *115*, 1661–1668.
- (68) Cämmerer, B.; Kroh, L. W. Antioxidant activity of coffee brews. *Eur. Food Res. Technol.* **2006**, *223*, 469–474.
- (69) Passos, C. P.; Kukurová, K.; Basil, E.; Fernandes, P. A.; Neto, A.; Nunes, F. M.; Murkovic, M.; Ciesarová, Z.; Coimbra, M. A. Instant coffee as a source of antioxidant-rich and sugar-free coloured compounds for use in bakery: Application in biscuits. *Food Chem.* **2017**, *231*, 114–121.
- (70) Hoelzl, C.; Knasmüller, S.; Wagner, K. H.; Elbling, L.; Huber, W.; Kager, N.; Ferk, F.; Ehrlich, V.; Nersesyan, A.; Neubauer, O.; et al. Instant coffee with high chlorogenic acid levels protects humans against oxidative damage of macromolecules. *Mol. Nutr. Food Res.* **2010**, *54*, 1722–1733.
- (71) Tang, C.; Li, X.; Li, Z.; Hao, J. Interfacial hydrogen bonds and their influence mechanism on increasing the thermal stability of nano-SiO₂-modified meta-aramid fibres. *Polymers* **2017**, *9*, 504.
- (72) Song, Pa.; Xu, Z.; Guo, Q. Bioinspired strategy to reinforce PVA with improved toughness and thermal properties via hydrogen-bond self-assembly. *ACS Macro Lett.* **2013**, *2*, 1100–1104.